Motion Representation of Ciliated Cell Images with Contour-Alignment for Automated CBF Estimation

Fan Zhang[1], Yang Song[1], Siqi Liu[1], Paul Young[2,3], Daniela Traini[2,3], Lucy Morgan[4,5], Hui-Xin Ong[2,3], Lachlan Buddle[4], Sidong Liu[1], Dagan Feng[1], and Weidong Cai[1]

[1] BMIT Research Group, School of IT, University of Sydney, Australia
[2] Woolcock Institute of Medical Research, Australia
[3] Discipline of Pharmacology, Sydney Medical School, University of Sydney, Australia
[4] Department of Respiratory Medicine, Concord Repatriation General Hospital, Australia
[5] School of Medicine, University of Sydney, Australia

Abstract. Ciliary beating frequency (CBF) estimation is of high interest for the diagnosis and therapeutic assessment of defective mucociliary clearance diseases. Image-based methods have recently become the focus of accurate CBF measurement. The influence from the moving ciliated cell however makes the processing a challenging problem. In this work, we present a registration method for cell movement alignment, based on cell contour segmentation. We also propose a filter feature-based ciliary motion representation, which can better characterize the periodical changes of beating cilia. Experimental results on microscopic time sequence human primary ciliated cell images show the accuracy of our method for CBF computation.

1 Introduction

Mucociliary transport is a major host defense that clears mucus and inhaled debris from human airways [1]. It depends on the coordinated beating of respiratory tract cilia to generate propulsive efforts for the continuous movement of mucus. Ciliary beating frequency (CBF) is a regulated quantitative function and has been widely used for measuring ciliary beating behaviors. CBF estimation plays an important role for the diagnosis of defective mucociliary clearance diseases, e.g., primary ciliary dyskinesia (PCD) that presents cilia with stationary or slow motion (CBF $<$ 11Hz) [2]. CBF can also assist the comparisons between external stimuli on increasing ciliary motility for therapeutic assessment [3].

In the last two decades, with the more advanced digital high speed imaging (DHSI) techniques, image-based CBF estimation has demonstrated its advantages over the traditional approaches such as photomultiplier and photodiode techniques [4,5]. First of all, DHSI can visualize the actual ciliary movement, instead of detecting light changes passing through the cilia. In this way, it enables the frame-by-frame manual observation by playing the images in a slow

N. Navab et al. (Eds.): MICCAI 2015, Part III, LNCS 9351, pp. 300–307, 2015.
DOI: 10.1007/978-3-319-24574-4_36

speed, which is considered a more accurate measurement but suffers from time consumption and observer fatigue issues. There have been methods that capture the ciliary movement by extracting temporal image signals such as intensity variation and optical flow [5,6,7]. These works provide the fundamentals for automated CBF computation. However, their automaticity is restricted by the fact that regions of interest (ROIs) above the cilia should be given in advance. In addition, the accuracy of these methods can be affected by the assumption that the temporal signal variations are only caused by displacements of cilia, without considering the issues of, e.g., illumination changes. Another limitation is that the ciliated cell where the cilia are closely packed can significantly influence the CBF measurement since the cell sometimes beats simultaneously and may obscure the observation of cilia. Recent studies attempted to remove the influence by incorporating cell alignment processing [8,9]. The methods, however, conducted the rigid registration considering the cell moves only in global translation and rotation manners. This could cause inaccurate estimation if a ciliated cell presents a local shape distortion. In addition, without the overall automated processing framework, the practicability of these methods is restricted.

In this study, we present an automated CBF estimation method using the microscopic time sequence ciliary images for more accurate CBF measurement. The main contributions are: 1) we proposed a contour-alignment process consisting of a non-rigid cell registration and cell contour segmentation, which can removing the influence of more complicated cell motion; 2) we extracted a filter-based motion representation feature, which is specified to characterize periodical motion of beating cilia; 3) we designed an automated CBF estimation framework without the manual beating cycle counting or ROI annotation. We tested our method on real human ciliary image data. The experimental results compared to the photomultiplier and manual observation approaches indicate that our method provides a substantial improvement for accurate CBF computation.

2 Ciliary Beating Frequency Estimation

2.1 Data Acquisition

Ciliary images were obtained from human primary ciliated epithelial cells. We collected the sample cells via nasal brushing and dislodged them into Medium 199. The sugar alcohol (mannitol) and β-agonist (salbutamol sulfate) were used to stimulate the cells within a 24-hour period. Ciliary images were then visualized with an Olympus IX70 microscope and captured using a Nikon D7100 camera. We tested our method on a set of 32 cases/movies with moving ciliated cells of various motions such as translation, rotation and shape distortion. For each case, we used 130 consecutive images of 720×1280 pixels for CBF computation, with a recording rate at 60 frames per second.

2.2 Region Division

We first segment the image into the ciliated cell, beating cilia and background regions, by identifying an outer contour C_{out} and inner contour C_{in}. The outer

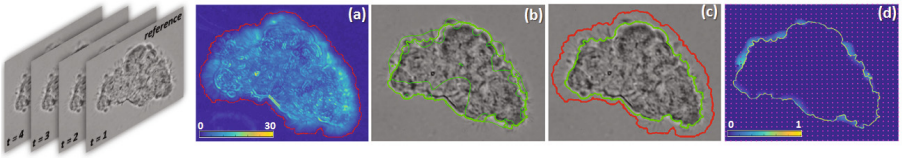

Fig. 1. Schema of cell segmentation and registration on an example image sequence: (a) C_{out} obtained given $ISDM$, (b) C_{in} computed with the DRLSE, (c) cilia region R_{cilia}, and (d) B-spline control point mesh and distance band weight.

contour C_{out} is used to separate the background. Considering that the cell and cilia can shift but background is still, we perform the segmentation on an intensity standard deviation map $ISDM$, as shown in Fig. 1(a). Given a position (x, y) in a time sequence of ciliary images $CI = \{I_t(x, y)|x \in [1, X], y \in [1, Y], t \in [1, T]\}$ with T images of size $X \times Y$, we extract its intensity curve along the time, and compute the intensity standard deviation $ISD(x, y)$. The map is then obtained as $ISDM = \{ISD(x, y)|x \in [1, X], y \in [1, Y]\}$. Due to the different moving behaviors, the cell and cilia regions present higher ISDs. We then use Sobel thresholding and extract the maximum connected component to segment the cell and cilia regions. A smoothing step is further performed to extend the contour to ensure that we include the entire cilia region.

Following that, the inner contour C_{in} is computed with a distance regularized level set evolution (DRLSE) [10] method to recognize the cell boundary. As the image sequence will be aligned to a reference $I_r \in CI$, we apply DRLSE on I_r with C_{out} as the initial segmentation. DRLSE obtains a sign matrix $\mathbf{S}$ corresponding to the level set formulation that takes negative values inside the zero level contour and positive values outside. We used the zero crossing points as C_{in}. DRLSE can also exhibit the cell contour as a signed distance band around the zero level set. The distance band can be used to weight the degree of motion of the nearby cell boundary areas. These areas normally show small beating motions, since the roots of cilia present less position displacement and become overlap with each other closer to the cell surface. This information will be incorporated into the cell registration for our contour-alignment processing.

2.3 Cell Registration

The aim of our cell registration is to ensure the observed motion of cilia only come from the ciliary beating. Hence, we do not want to over-emphasize the inside cell area nor, in particular, change the original ciliary beating behaviour, e.g., twisting the cilia based on those in the reference. The segmentation result can address these considerations by assigning higher priority to the cell boundary. Specifically, considering the cell movement mainly consists of non-rigid motions, we adopt the free-form deformation (FFD) [11] framework to get an aligned image sequence $CI' = \{I'_t|t \in [1, T]\}$ based on I_r (fixed as the first frame). FFD introduces high flexibility for local shape distortion to deform the cells while keeping the ciliary beating. It can also be naturally combined with the distance

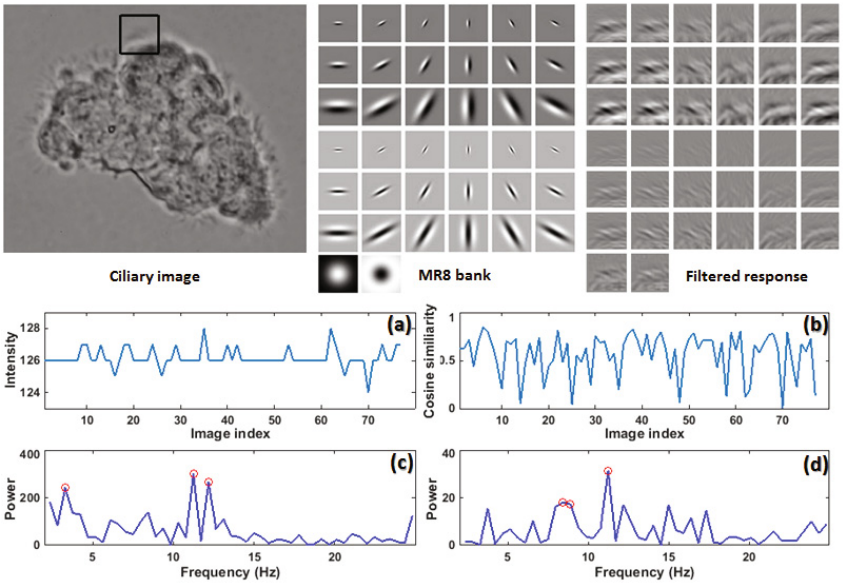

Fig. 2. Illustration of MR8-based signal extraction. The first row shows a visual representation of filtered responses given the 38 MR8 filters for a cilia ROI. The sub-figures (a) and (b) compare the original intensity and MR8 feature similarity curves for the middle position of the ROI, and (c) and (d) display the FFT frequency power distributions of the two signals, annotated with the first three dominant frequencies.

band for the contour alignment. Inspired by the work [12] that combines the structural boundary information with the textural intensity information, we incorporate the signed distance band from DRLSE for weighting the cell boundary area. The FFD with three levels of B-spline control points is implemented with the following energy function:

$$E(\mathbf{P}) = \sum((I_t(\mathbf{P}) - I_r(\mathbf{P})) \cdot w(C_{in}))^2 \tag{1}$$

$$w(x,y) = cosine(\frac{max(\mathbf{S}) - \mathbf{S}(x,y))}{max(\mathbf{S}) - min(\mathbf{S})}) \tag{2}$$

where $\mathbf{P}$ represents the B-spline control point matrix (the mesh window size is fixed at 20 for all experiments) and $\mathbf{S}$ is the sign matrix of DRLSE result. The weight $w(x,y) \in (0,1]$ gives priority to the control points in the middle of the band and gradually decreases towards the cilia and cell regions.

2.4 Ciliary Beating Signal Extraction

CBF is determined by timing a certain number of beating cycles, which is normally computed by capturing the recurrent displacement of cilia. Intensity variation is widely used in literature but can be influenced by noise, e.g., the illumination changes. In our method, after the cell registration, we apply a maximum

response 8 (MR8) filtering [13], which has proved effectively for image denoising, to highlight the periodical displacement of beating cilia. MR8 bank consists of 6 oriented edge and bar filters at 3 scales, and 2 isotropic filters ($6 \times 2 \times 3 + 2$, as shown in Fig. 2). The oriented filters that correspond to the directions of cilia can reinforce the ciliary motion description, and the isotropic filters can help illumination adaption. For each I'_t, we compute a 38-dimension MR8 feature vector $f_t(x, y)$ at position (x, y), and calculate a *cosine* similarity with $f_r(x, y)$ of I_r. Concatenating the similarities along the time, we obtain a signal curve $SC(x, y) = \{cosine(f_t(x, y), f_r(x, y))|t \in [1, T]\}$ to represent the periodical motion changes. A visual example after MR8 filtering is shown in Fig. 2. The cosine similarity curve (b) can better represent the periodical variations and thus result in a frequency power distribution with the more distinct dominant component (d), when compared to the original intensity curve (a and c).

2.5 Frequency Computation

Given the beating signal, we calculate the frequency with the FFT method for each position to obtain a whole field frequency map as processed by Sisson et al [5]. The frequencies from the region R_{cilia} between C_{in} and C_{out} are considered as our CBF estimation result. Post-processing to filter noise in the frequency spectrum [6] is also applied.

3 Experimental Results

Fig. 3 shows the visual results of region division and cell registration for a case in which the cell has non-rigid movement[1]. The outer and inner contours are annotated in red and green on the reference image in Fig. 3(a). It is worth noting that the segmentations need not be very accurate if we can find the approximate cell boundary that can keep all beating cilia out of the contour (please see the last paragraph of this section for details). For this reason, we manually adjusted the coefficient α for weighting the area term of DRLSE and fixed it as $\alpha = 1$[2] that generated a better overall performance.

Figs. 3(b) and (c) display the $ISDM$s given the original CI and aligned CI'. The ISDs from cell region of CI' were much lower, indicating the benefit of registration on removing the cell movement. For the target image in Fig. 3(d), Figs. 3(e) and (f) compare the FFD registration results without/with the distance band, given the same parameter settings. While both of them can properly align the target, our method resulted in smaller changes in the cilia region and hence could better keep the original ciliary beating behaviour. A quantitative comparison of mean ISD (MISD) across different registration approaches are listed

[1] Readers are recommended to refer to the supplementary examples for better visualization, if applicable.

[2] $\alpha = 1$ generated the optimal region division results for most cases but relatively shrinked the contours for the others. For other parameters involved in DRLSE, we followed the suggestions from the reference paper [10].

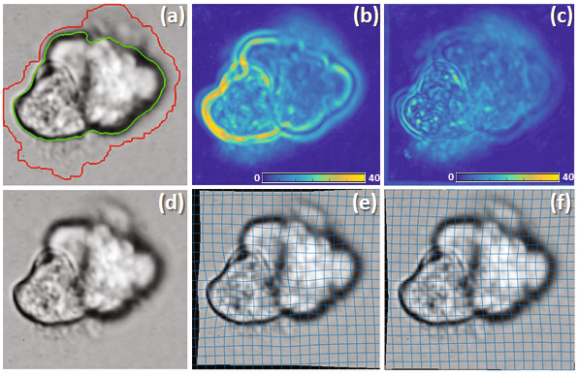

Fig. 3. Visual comparisons of the regions division and cell alignment results.

Table 1. Comparisons of MISDs across different registration methods.

	Original	Rigid	FFD	Proposed
Cell (inside C_{in})	9.67 ± 3.02	14.11 ± 6.67	**4.33** ± **2.01**	4.72 ± 2.26
Cilia (inside R_{cilia})	5.83 ± 1.91	17.42 ± 9.53	**4.16** ± **1.71**	4.23 ± 1.80
Distance band ($w > 0.5$)[3]	11.8 ± 3.76	12.38 ± 7.51	6.16 ± 3.39	**5.62** ± **3.71**

in Table 1, including a rigid intensity-based registration with gradient descent optimization, the original FFD and our method. The rigid registration obtained higher MISDs than the non-rigid registrations. Compared to the original FFD method, we obtained higher MISDs for the cell and cilia regions but smaller values in the distance band area. These results are due to that our method incorporated the weighting scheme in Eq. (2), which assigned higher priority to the control points located nearby the cell boundary. A better registration of this region could remove the influence of moving cell and keep the original ciliary beating behaviour to a large extent, and hence is more desirable even at some expense of the registration performance for the cell and cilia.

Fig. 4 illustrates the CBF estimation results given different signals. For the intensity variations, although the cell registration was incorporated in CI', the difference from CI was small. The more observable changes can be found with the MR8 feature-based signals. Firstly, the beating frequencies from the cell region were largely reduced. The higher frequencies that are usually considered originating from the beating cilia are thus more distinguishable. This can explain why a smaller cell contour has relatively negligible influence on our CBF computation. In addition, with the combination of registration and filtering, we can provide a more accurate CBF estimation. For example of the first case, given the area circled in white that contains a cluster of immotile cilia, the first two approaches failed to recognize them. The third method obtained a lower frequency spectrum that however was from the movement of ciliated cell. Our method gave the best estimation result.

[3] $w > 0.5$ gave a more suitable range of cell boundary and was thus selected. For other parameters of FFD, we followed the suggestions from the reference paper [11].

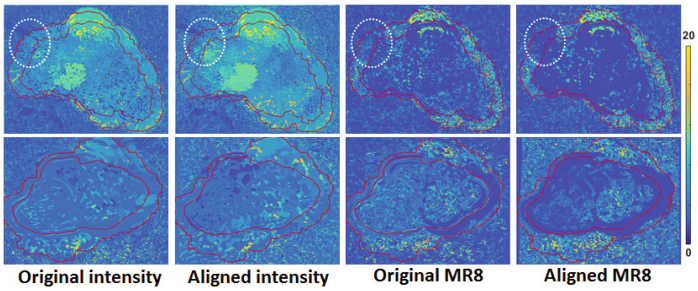

Fig. 4. Comparisons of the whole field frequency maps given different signals.

Table 2. Comparisons of MSE and MD with MO and PM estimations.

		Original intensity	Aligned intensity	Original MR8	Aligned MR8
MSE	Cell	6.216	6.135	4.217	**2.311**
	Back	4.650	5.517	**2.928**	3.701
	Cilia	7.575	7.188	5.999	**5.356**
MD	Avg	0.131	0.130	0.156	**0.551**
	SD	0.670	1.101	2.413	**2.771**
	Max	4.700	5.938	8.739	**9.609**

We conducted the manual observation (MO) estimation for quantitative performance comparison. For each case, we randomly sampled 10 points from each cell, cilia and background regions. For the cell and background points, the frequencies were set as 0Hz; for the cilia points, we conducted frame-by-frame observation to time 10 beating cycles, in terms of the relative position displacement between the cilia and nearby cell boundary. The mean square errors (MSEs) of the frequencies of these points between the MO and the various methods are listed in Table 2. With our method (Aligned MR8), the smallest difference can be observed in the cell region, showing the benefits of our contour-alignment process. Our method also obtained the best correlation with the MO estimation for the cilia region. To further validate the CBF measurement, we also compared our result with the photomultiplier (PM) approach. The PM method captured the electronic signals from the photometer through an oscilloscope and documented the signals with Mac-Lab recording system. Given the average (Avg), standard deviation (SD) and maximum (Max) of frequencies in the cilia region from the PM estimation, we report the mean difference (MD) of the statistics of our method in Table 2. The results using the original intensity method were the most similar to PM, since they shared the same signal source from the moving cell. The MR8-based approaches obtained larger MDs, but corresponded to the smaller MSEs from the MO estimation. This observation indicates that the periodical changes of beating cilia, which were essential for CBF estimation, were better characterized by the MR8 features compared to PM and the original intensity. We also suggest that the cell alignment is more important if we focus on a certain cilia region, e.g., recognizing the immotile cilia as shown in Fig. 4.

4 Conclusions

We present an image-based method for CBF estimation, based on the region division, ciliated cell registration and the signal extraction. Our method can provide a more accurate ciliary motion representation by removing the influence from the moving cell. With the MR8 feature we can better represent the periodical motion of beating cilia from the non-cilia objects. Our estimation results are expected to be more suitable for diagnosing the defective mucociliary clearance and observing the therapeutic effects of different drugs. The method also provides an alternative for the conventional CBF measures in an automated way, which avoids the time-consuming and high-cost processing.

References

1. Wanner, A., Salathé, M., et al.: Mucociliary clearance in the airways. American Journal of Respiratory and Critical Care Medicine 154(6), 1868–1902 (1996)
2. Stannard, W.A., Chilvers, M.A., et al.: Diagnostic testing of patients suspected of primary ciliary dyskinesia. American Journal of Respiratory and Critical Care Medicine 181(4), 307–314 (2010)
3. Salathe, M.: Effects of β-agonists on airway epithelial cells. Journal of Allergy and Clinical Immunology 110(6), S275–S281 (2002)
4. Chilvers, M.A., O'Callaghan, C.: Analysis of ciliary beat pattern and beat frequency using digital high speed imaging: comparison with the photomultiplier and photodiode methods. Thorax 55(4), 314–317 (2000)
5. Sisson, J.H., Stoner, J.A., et al.: All-digital image capture and whole-field analysis of ciliary beat frequency. Journal of Microscopy 211(2), 103–111 (2003)
6. Smith, C.M., Djakow, J., et al.: ciliaFA: a research tool for automated, high-throughput measurement of ciliary beat frequency using freely available software. Cilia 1(14), 1–7 (2012)
7. Kim, W., Han, T.H., et al.: An automated measurement of ciliary beating frequency using a combined optical flow and peak detection. Healthcare Informatics Research 17(2), 111–119 (2011)
8. Parrilla, E., Armengot, M., et al.: Optical flow method in phase-contrast microscopy images for the diagnosis of primary ciliary dyskinesia through measurement of ciliary beat frequency. Preliminary results. In: ISBI, pp. 1655–1658 (2012)
9. Zhang, F., et al.: Image-based ciliary beating frequency estimation for therapeutic assessment on defective mucociliary clearance diseases. In: ISBI, pp. 193–196 (2014)
10. Li, C., Xu, C., et al.: Distance regularized level set evolution and its application to image segmentation. IEEE Trans. Imag. Process. 19(12), 3243–3254 (2010)
11. Rueckert, D., Sonoda, et al.: Nonrigid registration using free-form deformations: application to breast MR images. IEEE Trans. Med. Imag. 18(8), 712–721 (1999)
12. Myronenko, A., Song, X., Sahn, D.J.: LV motion tracking from 3D echocardiography using textural and structural information. In: Ayache, N., Ourselin, S., Maeder, A. (eds.) MICCAI 2007, Part II. LNCS, vol. 4792, pp. 428–435. Springer, Heidelberg (2007)
13. Varma, M., Zisserman, A.: Classifying images of materials: achieving viewpoint and illumination independence. In: Heyden, A., Sparr, G., Nielsen, M., Johansen, P. (eds.) ECCV 2002, Part III. LNCS, vol. 2352, pp. 255–271. Springer, Heidelberg (2002)